INTERNATIONAL JOURNAL FOR NUMERICAL METHODS IN FLUIDS
*Int. J. Numer. Meth. Fluids* 2008; **56**:1107–1113
Published online 22 January 2008 in Wiley InterScience (www.interscience.wiley.com). DOI: 10.1002/fld.1719

# Numerical simulation of generic side mirror of a car using large eddy simulation with polyhedral meshes

I. Afgan[1,*,†], C. Moulinec[2] and D. Laurence[2]

[1]*Institute of Avionics and Aeronautical Engineering, Air University, Islamabad, Pakistan*
[2]*School of Mechanical, Aerospace and Civil Engineering, University of Manchester, Manchester M60 1QD, U.K.*

SUMMARY

The flow structure around a generic side mirror of a car is numerically investigated via large eddy simulation (LES) incorporating polyhedral meshes. The aspect ratio defined as height to radius of the cylinder is 3 and the Reynolds number based on cylinder diameter and free stream velocity is $3.2 \times 10^5$. The aim of the current paper is not only to show the advantage of the use of polyhedral mesh to model the generic car mirror via LES but also to obtain fluctuating pressure spectra for noise prediction. LES has been an obvious choice for the simulation as it is very suitable for bluff body flows with small effects of boundary layers. It is easier, more flexible and far less time consuming to mesh the current geometry using unstructured mesh rather than a structured conforming mesh. However, central differencing scheme holds better kinetic energy conservation properties on polyhedral cells than on non-conforming tetrahedral cells. Three different grids were tested with local prismatic layer refinements near solid walls. The flow was found to be fully three dimensional with an upstream laminar separation. The stagnation point was located at zero degrees for both the cylinder and the sphere. Pressure spectra were monitored at particular locations upstream of the body and in its wake. Copyright © 2008 John Wiley & Sons, Ltd.

Received 30 April 2007; Revised 14 November 2007; Accepted 15 November 2007

KEY WORDS: acoustics; incompressible; large eddy simulation; polyhedral meshes; separation; stagnation

## 1. INTRODUCTION

Over the years the modern automobiles have transformed from simple transportation devices to comfortable luxury vehicles. This transformation has gone through a lot of changes; improvements in vehicle control, reduction in manufacturing cost, passenger safety, ergonomics and passenger

*Correspondence to: I. Afgan, Institute of Avionics and Aeronautical Engineering, Air University, Sector E-9, Islamabad, Pakistan.
†E-mail: afgan_imran@hotmail.com, imran.afgan@mail.au.edu.pk

comfort. Although for a typical car the main source of noise generation is the engine itself, however, any extremities such as side mirrors have a significant impact in the total noise generation. From a performance point of view the contribution of a generic side mirror to total drag of a car is around 3–6% [1]. From an acoustic point of view interesting studies are of [2, 3], where the authors test a full-scale car model. However, from a general point of view the experimental data seem somewhat redundant due to use of specific mirror geometry and a full-scale car model. As compared with [2, 3] a more generic side mirror shape was numerically studied by Rung *et al*. [4] in which the authors compare DES with unsteady Reynolds-averaged Navier–Stokes at a moderate *Re* number of $5.2 \times 10^5$. A more detailed DES and large eddy simulation (LES) comparison was done by Ask and Davidson [5] concluding that LES showed marked improvement over DES in terms of pressure fluctuation levels (PFLs); however, the mirror mean surface pressure values were still found to be comparable by the two numerical techniques. The aforementioned studies of [4, 5] both use the experimental and numerical data of [6, 7].

## 2. CASE DESCRIPTION AND NUMERICS

The generic car mirror mounted on a flat plate consists of a half cylinder complemented by a quarter sphere at the tip. The aspect ratio ($AR = H/R$) of the mirror geometry is 3 with radius being 0.1 m. The inlet velocity is fixed at 26 m/s and the corresponding *Re* number is $3.2 \times 10^5$. For the simulations no artificial perturbations are prescribed at the inlet. Owing to the complex shape of the geometry, a totally conforming regular mapped mesh would have been too complex and computationally very expensive. Alternative solution could have been a tetrahedral mesh. However, this would have resulted in a huge number of cells especially since tetrahedral are the most simplest of elements and can hence not be stretched too much. Thus, polyhedral mesh was generated in individual blocks and was later assembled by multi-block transformation technique. Three different grids were used as shown in Table I. For the coarse mesh (CM) and medium mesh (MM) the geometry is wrapped around by a single fine mesh (FM) block, which progressively becomes coarser as we move away from the mirror body. For the FM two encapsulating blocks are used; fine block (FF1) and a very fine block (FF2) inside FF1. An inter-dependant boundary layer meshing technique is used utilizing a prism layer of regular orthogonal cells containing at least 20 cells in wall normal direction. For the FM near the mirror surface viscous sub-layer is assumed to be resolved, where the $Y^+$ is close to 1. For this FM the prism layer spans till $Y^+ = 90$ for the mirror body, whereas it covers around $Y^+ = 54$ in the immediate wake of the mirror. However, no attempt has been made to resolve the boundary layer over the flat plate as this would have increased the computational requirements considerably. The flow was assumed to be Newtonian and incompressible, whereas the solver used was the prototype version of CD-Adapco's STAR-CD V4.

Table I. Size of computational grids and encapsulating blocks in millions.

| Mesh | Cells | Nodes | Faces | No. of inner encapsulating blocks |
|---|---|---|---|---|
| CM | 0.4 | 1.4 | 2.0 | 1 (CF1, 0.25) |
| MM | 0.8 | 4.0 | 5.0 | 1 (MF1, 0.50) |
| FM | 1.9 | 8.8 | 11.2 | 2 (FF1, 0.45) and (FF2, 0.55) |



DOI: 10.1002/fld

For LES the filtered continuity and Navier–Stokes equations are given as follows:

$$\frac{\partial \overline{u}_i}{\partial x_i}=0, \quad \frac{\partial \overline{u}_i}{\partial t}+\frac{\partial \overline{u}_i \overline{u}_j}{\partial x_j}=-\frac{1}{\rho}\frac{\partial \overline{p}}{\partial x_i}+\nu\frac{\partial^2 \overline{u}_i}{\partial x_j \partial x_j}-\frac{\partial \tau_{ij}}{\partial x_j}, \quad i\in\{1,2,3\} \tag{1}$$

where $\tau_{ij}=-2\nu_t \overline{S}_{ij}$. For the subgrid-scale modelling, the standard Smagorinsky model $\nu_t=2(C_S\overline{\Delta})^2\|S\|$ is used, where $\overline{S}_{ij}$ is the filtered strain rate tensor ($\|S\|=\sqrt{2\overline{S}_{ij}\overline{S}_{ij}}$). The filter width in the above formulation is taken to be twice that of the cube root of the cell volume ($\overline{\Delta}=2\,\mathrm{Vol}^{1/3}$). The Smagorinsky constant ($C_S$) is set to 0.065 and is locally damped by a Van Driest wall damping function near solid walls. For spatial discretizations second-order central differencing scheme is used whereas pressure–velocity coupling is ensured by a prediction/correction method using the SIMPLEC algorithm, [8] also described in [9]. For time discretizations three time-level implicit time-advancing scheme of [9] is used with a time step of $2.5\times10^{-4}$ s. The simulation was run on 10 Pentium 4 dual core machines in parallel with a total CPU time of around 100 h. The total simulation time on the other hand was 18 s where collection of statistics was done over the last 12 s to ensure adequate time averaging of flow parameters. In the far field where the grid is considerably coarse and is of no direct interest, to avoid artificial numerical wiggles [9] the second-order central scheme has been blended with the first-order upwinding.

## 3. RESULTS AND DISCUSSIONS

Tetrahedral cells only have four neighbours that can in some cases lead to problems while computing gradients along cell centres. Near corners cells might end up with only two or at times even one neighbour, which could lead to serious numerical instabilities. Polyhedral cells, on the other hand, have a lot of neighbours probably around 10 or more, which allows for reasonable predictions of both gradients at cell centres and local flow directions. However, on a negative side more neighbours for every cell mean a higher storage space and computing requirement but local tests and the ones conducted at CD-Adapco [10] confirm that the added computing expenditure is more than compensated by the higher accuracy and quick convergence of results. Second-order accuracy is retained for polyhedral meshes much like Cartesian structured grids for simple approximations such as mid-point rule and linear interpolation. For tetrahedral meshes, on the other hand, special approximations are required to hold equally good accuracy [10]. The conservation of kinetic energy is a critical issue for any DES or LES, addressed in detail by Benhamadouche and Laurence [11] for unstructured meshes. Indeed polyhedral meshes (considered to be unstructured meshes) need to behave in a similar fashion. Peric [10] and Moulinec *et al.* [12] show that polyhedral meshes hold kinetic energy conservation far superior than tetrahedral meshes. Moulinec *et al.* [12] test polyhedral meshes for a U-bend and shows good comparison with experimental data. For such a configuration a regular Cartesian grid is hard to generate taking into consideration the cell stretching close to outer walls near the bend. Peric [10] shows more basic tests on retaining kinetic energy over a flat two-dimensional surface. Results indicate the same that polyhedral meshes conserve kinetic energy much like the Cartesian hexahedral meshes but with much lower number of cells (approximately half). For the current case the Mach number is 0.08 and hence incompressibility can be assumed with reliability since both experiments and numerical simulations performed at a slightly higher Mach number of 0.11 also hold this condition true [4–6]. The flow over generic car mirror is an open vortex flow with a laminar upstream separation. The approaching flow is seen to



DOI: 10.1002/fld

be fully symmetrical with no variance in the flow incidence angle. The stagnation point is located at zero degrees for both the cylinder and the sphere bodies. The laminar separation can best be seen by the oil flow visualizations of the experiments shown in Figure 1(a), which is taken from [5]. The measurements are at an *Re* number of $5.2\times10^5$ and the separation line is located 0.15 D upstream of the mirror edge. Figure 1(b) shows the wall shear stress from the LES simulation of the FM for a slightly lower *Re* number of $3.2\times10^5$. Interestingly, the simulations predict the location to be 0.1525 which is an excellent comparison given the slightly lower *Re* number. LES of [5] shown in Figure 1(c) still predicts a fair location of 0.1 D. The mean flow as a whole decelerates as it approaches the cylinder part of the mirror. However, the spherical shape of the mirror tip helps the flow to accelerate that adds to the deflection of mean flow causing a single large open vortex in the mirror wake. The deflected acceleration also increases the mean flow velocity by 30–40% near the mirror tip. The mean flow over the mirror geometry does not exhibit regular vortex shedding because of a very small AR, thus the wake is dominated by a single large vortex coming from the top of the mirror. The reattachment point of this vortex in the mirror wake is 2.5 D as suggested by the experimental results. For the LES (FM) the normalized mean streamwise '$u$' and normal '$v$' velocities along the centre plane ($Y/R=0$) in the mirror wake are shown in Figure 2(a). One notices that the normal velocity tends to zero at approximately 2.75 D downstream of the mirror, which is a fair agreement with experiments. In Figure 2(b) the normalized mean velocity profiles are shown along certain lines. The numerically predicted location of horseshoe vortex is 0.95 D (1.9 R) in the spanwise ($Y$) direction also shown as dashed horizontal line in Figure 2(b) (the concave curve at this particular location for top profile ($Z/R=0.1$)). Interestingly, the experimental measurements show this location to be 0.925 D in the spanwise direction which is once again an excellent match. An instantaneous realization of the second invariant of the velocity gradients for LES (FM) is shown in Figure 3. For computations, $Q$ is defined as $Q=-0.5[S_{ij}S_{ij}-\Omega_{ij}\Omega_{ij}]$ [13]. Herein it is normalized as $(Q=\alpha(U_0/L_C)^2)$ where $\alpha$ is a non-dimensional constant set to return

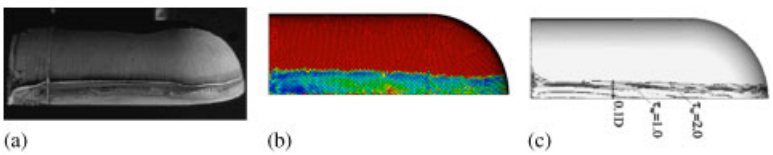


Figure 1. Separation line location: (a) oil flow visualizations; (b) LES (FM); and (c) LES [5].

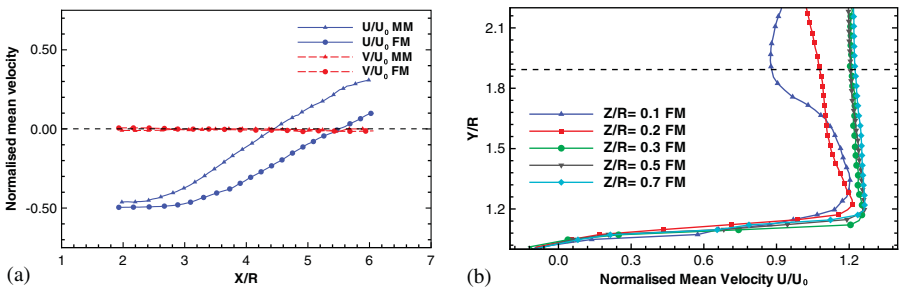


Figure 2. Normalized mean velocity profile: (a) reattachment point and (b) horseshoe vortex location.



DOI: 10.1002/fld

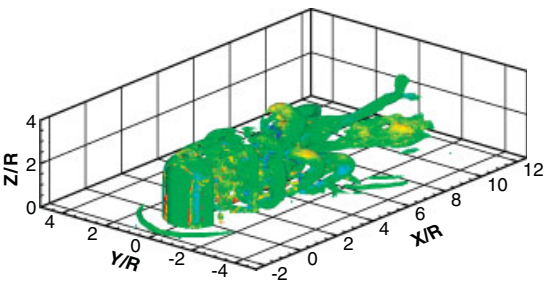


Figure 3. Instantaneous realization of Iso-Q.

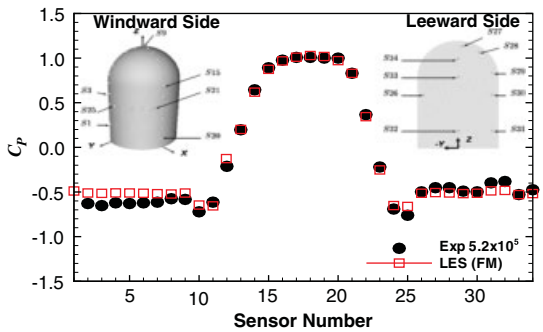


Figure 4. $C_p$ profile at selected stations.

a value of $Q=1$. For the Iso-Q structures shown in Figure 3 one notices not only the existence and location of horseshoe vortex but also the fine and large structures in the mirror wake. To measure the mean pressure on the cylinder surface a number of sensor locations were predefined. The LES and experimental mean pressure profiles ($C_P$) and the actual sensor locations are shown in Figure 4, where ($C_P$) is defined as $C_P=2(P-P_{\text{ref}})/\rho U_0^2$ and the reference pressure $P_{\text{ref}}$ is set to zero. Since the sensors 1–9 lie downstream of the separation zone, they show a constant $C_P$ profile. On the other hand, sensors 10–11 and 24–25 actually lie just before this separation zone and hence show a slight dip in $C_P$ profile. Sensors 12–23 lie on the front side of the mirror and hence show an increase in $C_P$ values. The stagnation region is also evident from this curve which is shown by the constant $C_P=1$ value for sensors 16–20.

The aero-acoustic analyses for a noise generating object present in a flow field was initially proposed by Lighthill [14]. To account for the presence of solid walls, Curle [15] and then later Ffowcs and Hawkings [16] proposed modifications to Lighthill analogy. These analogies convert the governing equation of continuity and momentum to an inhomogeneous wave equation containing monopole, dipole and quadrapole source terms. For a stationary surface the monopole term vanishes. When Mach number is low ($Ma<0.2$) the contribution of the quadrapole term is less than 0.01% and hence can also be ignored [17]. The effective term thus left is the dipole term which can be expressed in terms of PFLs as $\text{PFL}(y)=20\log_{10}(p_{sf}(y,t)_{\text{rms}}/p_0)$, where $y$ is the surface location where the pressure fluctuations are being monitored. The reference pressure $p_0$ is set to $2.0\times10^{-5}$ Pa. PFL along with pressure fluctuations for three different locations are



DOI: 10.1002/fld

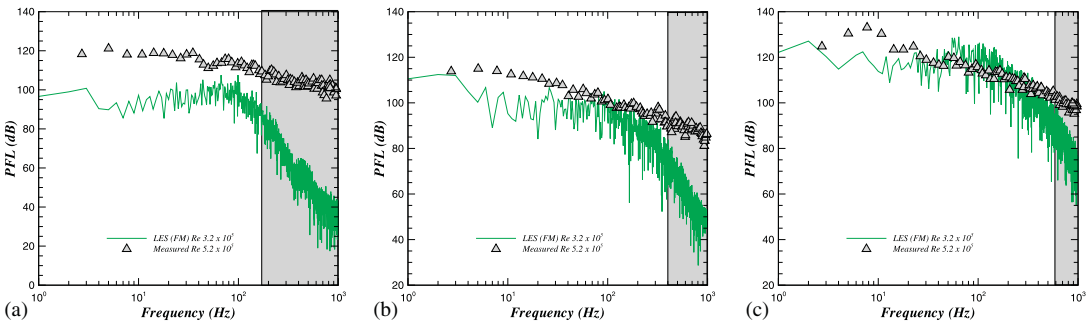


Figure 5. PFL on flat plate: (a) sensor 116; (b) sensor 119; and (c) sensor 123.

computed and are shown in Figure 5. The sensors 116 and 119 are both located on the centreline in the $XZ$ plane on the surface of the flat plate at $X=-0.6\,\mathrm{D}$ and 1 D, respectively. The sensor 123 is, however, located at $X=2.489\,\mathrm{D}$ and $Y=0.709\,\mathrm{D}$. These locations were chosen from the experimental data of [6, 7], which is also shown as a comparison in Figure 5. Acoustic data were collected for 12 s which corresponds to a data set of 48 000 values for every sensor location. The numerically computed PFL compare quite well to the measured profiles where a slightly lower prediction is due to the *Re* number being slightly lower for the computations. Since the experimental data is at a much higher *Re* number of $5.2\times10^5$, the numerical data can be translated by 8.5 dB which is in accordance with the *Re* number adjustment.

## 4. CONCLUSIONS

In the current study an attempt was made to fully investigate the flow behaviour over a generic car mirror. Incompressibility was assumed for all simulations since the Mach number is sufficiently small. Polyhedral cells were used for the first time with LES on such a complex geometry to test its capabilities. The flow field was found to have a laminar separation 0.1525 D upstream of the leeward side of the mirror. The flow shows almost no classical Karman vortex shedding due to very small AR. Furthermore, in the close vicinity of the mirror tip the local flow field is seen to increase in velocity by around 30–40%. The reattachment point for the flow is located at around 2.75 D in the mirror wake. The interaction of the classical pillar plate junction is also observed in the form of a horseshoe vortex which is located 0.95 D away from the body in both streamwise and spanwise directions. The PFLs were also computed at three different locations and were found to be in fair agreement with the experimental measurements.

## REFERENCES

1. Barnard RH. *Road Vehicle Aerodynamic Design*. Longman: New York, 1988.
2. Ono K, Himeno R, Fukushima T. Prediction of wind noise radiated from passenger cars and its evaluation based on auralization. *Journal of Wind Engineering and Industrial Aerodynamics* 1999; **81**:403–419.
3. Watkins S, Oswald G. The flow field of automobile add-ons, with particular reference to the vibration of external mirrors. *Journal of Wind Engineering and Industrial Aerodynamics* 1999; **83**:532–554.
4. Rung Th, Eschricht D, Yan J, Thiele F. Sound radiated of the vortex flow past a generic side mirror. *Proceedings of the 8th AIAA/CEAS Conference*, Colorado, U.S.A., 2002.



DOI: 10.1002/fld

5. Ask J, Davidson L. The sub-critical flow past a generic side mirror and its impact on sound generation and propagation. *Proceedings of the 12th AIAA/CEAS Conference*, MA, U.S.A., 2006.
6. Hold R, Brenneis A, Eberle A, Schwarz V, Siegert R. Numerical simulation of aerodynamic sound generation by generic bodies placed on a plate: part I—prediction of aerodynamic sources. *Proceedings of the 5th AIAA/CEAS Conference*, *AIAA-99-1896*, Washington, U.S.A., 1999.
7. Siegert R, Schwartz V, Reichenberger J. Numerical simulation of aerodynamic sound generation by generic bodies placed on a plate: part II—prediction of radiated sound pressure. *Proceedings of the 5th AIAA/CEAS Conference, AIAA-99-1895*, Washington, U.S.A., 1999.
8. Van Doormal JP, Raithby GD. Enhancements of the SIMPLE method for predicting incompressible fluid flows. *Numerical Heat Transfer* 1984; **7**:147–163.
9. Ferziger JH, Peric M. *Computational Methods for Fluid Dynamics* (3rd edn). Springer: Berlin, 2002.
10. Peric M. Flow simulation using control volumes arbitrary polyhedral shape. *ERCOFTAC* 2004; **62**:25–29.
11. Benhamadouche S, Laurence D. Global kinetic energy conservation with unstructured meshes. *International Journal of Numerical Methods* 2002; **40**:561–572.
12. Moulinec C, Benhamadouche S, Laurence D, Peric M. LES in a U-bend pipe meshed by polyhedral cells. *Proceedings of ERCOFTAC Conference*, Sardinia, 2005.
13. Hunt JCR, Wray AA, Moin P. Eddies, stream and convergence zones in turbulent flows. *Report CTR-S88*, Center for Turbulent Research, 1988.
14. Lighthill MJ. On sound generated aerodynamically. *Proceedings of the Royal Society of London*, *Series A* 1952; **A211**:564–587.
15. Curle N. The influence of solid boundaries upon aerodynamic sound. *Proceedings of the Royal Society of London*, *Series A* 1955; **A231**:505–514.
16. Ffowcs WJ, Hawkings D. Sound generation by turbulence and surfaces in arbitrary motion. *Philosophical Transactions of the Royal Society* 1969; **A264**:321–342.
17. Grahs T, Othmer C. Evaluation of aerodynamic noise generation: parameter study of a generic side mirror evaluating the aeroacoustic source strength. *Proceedings of ECCOMAS Conference*, The Netherlands, 2006.



DOI: 10.1002/fld